RESEARCH Revista Mexicana de Física **66** (1) 35–41 JANUARY-FEBRUARY 2020

A theoretical study of variation of photoionization cross section of donor impurities in a GaAs quantum dot of cylindrical geometry with incident photon frequency, donor location along the dot axis and applied uniaxial stress

F. Oketch[a,b] and H. Oyoko[a,*]
[a]*Department of Physics, Pwani University, Kilifi 195-80108, Kenya.*
**e-mail: h.oyoko@pu.ac.ke*
[b]*Department of Mathematics and Physics, Technical University of Mombasa, Mombasa 90420-80100, Kenya.*

Received 19 June 2019; accepted 19 July 2019

In this work, we have used a variational technique within the effective mass approximation to study the variation of the photoionization cross section of a donor impurity in a cylindrical GaAs quantum dot with incident photon frequencies and applied uniaxial stress. We have used the dipole approximation and assumed that the barrier potential is infinite. Our results show that the photoionization cross section begins at a finite value and increases with increasing frequency until it reaches a peak and then it decreases gradually, almost exponentially, until it reaches a finite value when it is almost insensitive to any further increase in frequency. Furthermore, for a particular quantum dot length, the photoionization cross section decreases with increasing applied uniaxial stress. We have also noted that the longer the quantum well dot, the larger is the photoionization cross section.

Keywords: GaAs quantum dot; photoionization cross section; hydrogenic donor impurity; non hydrogenic donor impurity; uniaxial stress.

PACS: 73.21- b; 73.21 La

DOI: https://doi.org/10.31349/RevMexFis.66.35

1. Introduction

The invention and development of new techniques for fabricating semiconductor nanostructures [1-5] have made it possible to design quantum wells, quantum well wires and quantum dots of various cross-sections. Of these, one semiconductor material that has been of great interest for device application is Gallium Arsenide (GaAs). The GaAs has been studied extensively both experimentally and theoretically [6-14]. These studies have been directed towards determining its potential for optical and electronic device applications. In this regard, the GaAs quantum well dot is of particular interest. This is, essentially, an object with zero spatial dimensions. The quantum well dot comes in cylindrical, rectangular, triangular and, some other quite esoteric geometries. Studies have been carried out on donor impurity binding energies in GaAs quantum wells [14,15], quantum well wires [16] and quantum dots [17-19]. Further work has seen the use of the binding energies to compute density of impurity states [9] and photoionization cross-sections [20-26] when the system is subjected to external constraints. In our previous work [26], we have studied the effect of Hermanson's spatial dielectric function, finite and infinite barrier potentials and axial lengths on the photoionization cross-section of a hydrogenic and a non-hydrogenic donor impurity in a GaAs quantum well dot (QWD) of circular cross-section. We found that the photoionization cross-section of the hydrogenic donor impurity is much larger than that of the non-hydrogenic donor impurity in the same frequency range and in the finite and the infinite barrier potential regimes.

In the present work, we have considered a hydrogenic donor impurity located at different axial positions in a GaAs quantum dot (QD) of cylindrical geometry. We have carried out a theoretical study of the variation of the photoionization cross-section of the donor impurity with incident photon frequency, the location of the donor impurity along the axis of QD and applied uniaxial stress. In the study, we calculated the donor impurity binding energies as functions of the location of the donor impurity along the axis of the QD, incident photon frequency and applied uniaxial stress. We then used the binding energies to calculate the photoionization cross-sections of the donor impurity when the system is subjected to various incident photon frequencies, applied uniaxial stress and for various locations of the QD axis. In our calculations we have used a variational technique within the effective mass and dipole approximations [26,27]. It should, however, be noted that other works [28-30] have employed other techniques such as spin density functional theory instead of the variational technique to carry out similar studies. We have assumed that a $\mathrm{Ga}_{1-x}\mathrm{Al}_x\mathrm{As}$ matrix surrounding the GaAs QD provides an infinite potential barrier.

Our work is organized as follows: In Sec. 2 we present the theoretical framework, while in Sec. 3 we present the results and discussions. Finally, in Sec. 4 we give our conclusions.

2. Theoretical model

2.1. Hydrogenic Donor Impurity

The Hamiltonian for a hydrogenic donor impurity which is located along the QD axis is given by

$$H_h = -\frac{\hbar^2}{2m^*(p)}\left\{\frac{1}{\partial}\frac{\partial}{\partial\rho}\left(\rho\frac{\partial}{\partial\rho}\right)+\frac{\partial^2}{\partial z^2}\right\} - \frac{e^2}{4\pi\varepsilon(p)[\rho^2+(z-z_i)^2]^{1/2}} + V_B(\rho,z,P), \quad (1)$$

where, $m^*(P)$ is the stress dependent effective mass of the donor impurity in the QD and $\varepsilon(P)$ is the stress-dependent dielectric function. The position of the donor impurity is given by

$$r = [\rho^2 + (z - z_i)^2]^{1/2}. \quad (2)$$

In Eq. (1),

$$m^*(P)=\left\{1+E_P^\Gamma\left[\frac{2}{E_P^\Gamma(P)}+[E_P^\Gamma(P)+\Delta_0]^{-1}\right]\right\}^{-1} m_e, \quad (3)$$

where m_e is the mass of the free electron [31-33], $E_P^\Gamma = 7.51$ eV is the energy related to the momentum matrix element, $\Delta_0 = 0.341$ eV is the spin-orbit splitting energy. E_P^Γ is the uniaxial stress-dependent energy gap for GaAs QD semiconductor at the Γ-point in units of eV [34].

$$E_P^\Gamma(P) = a + bP + cP^2, \quad (4)$$

where $a = 1.425$ eV, $b = 1.26 \times 10^{-2}$ eV/(kbar), $c = -3.77 \times 10^{-5}$ eV/(kbar)^2 and $E_P^\Gamma(0) = 1.519$ eV is the energy gap for the GaAs QD at the Γ-point when the uniaxial stress is $P = 0$ kbar. In Eq. (1), the stress-dependent dielectric constant is given by [31-33]

$$\varepsilon(P) = \varepsilon(0)\exp(\delta P), \quad (5)$$

where, $\varepsilon(0) = 12.56$ is the static dielectric constant of GaAs, [13] and $\delta = -1.73 \times 10^{-3}$ kbar.

In Eq. (1),

$$V_B(\rho,z,P)=V_B(z,P)=\begin{cases} 0, & |z| \le \frac{L_z(P)}{2} \\ V_0(P), & |z| > \frac{L_z(P)}{2} \end{cases}, \quad (6)$$

is the barrier potential which confines the donor impurity within the quantum dot. In this equation, $L_z(P)$ is the stress-dependent length of the QD and $V_0(P)$ is the barrier height as a function of the applied stress. These are given by,

$$L_z(P) = L_z(0)[1 - (S_{11} + 2S_{12})P] \quad (7)$$

and

$$V_0(P) = Q_c \Delta E_g^\Gamma(x,P), \quad (8)$$

where in Eq. (7), $S_{11} = 1.16 \times 10^{-3}$ (kbar)$^{-1}$ and $S_{12} = -3.7 \times 10^4$ (kbar)$^{-1}$ and $L_z(0)$ is the unstrained length of the QD. In Eq. (8), $Q_c = 0.658$ is the band offset parameter, while $\Delta E_g^\Gamma(x,P)$ is the band gap difference between the QD material and the barrier material and is given by

$$\Delta E_g^\Gamma(x,P) = \Delta E_g^\Gamma(x) + PD(x), \quad (9)$$

where in the above equation, $\Delta E_g^\Gamma(x) = (1.15x + 0.37x^2)$ eV gives the variation of energy gap difference in the absence of the applied stress, while the quantity $D(x) = [-(1.3\times10^{-3})x]$ eV/kbar is the stress coefficient of the band gap. Our trial wave function for the hydrogenic donor impurity in its ground state is given by

$$\Psi_i(\rho,z) = N_i J_0(\alpha\rho)\cos(\beta z) \times \exp\left\{-\lambda[\rho^2 + (z - z_i)^2]^{1/2}\right\}. \quad (10)$$

Thus, the kinetic energy is found as follows,

$$H_T\Psi_i(\rho,z)=-\frac{\hbar^2}{2m^*(P)}\left\{\frac{1}{\rho}\frac{\partial}{\partial\rho}\left(\rho\frac{\partial}{\partial\rho}\right)+\frac{\partial^2}{\partial z^2}\right\}\Psi_i(\rho,z)=-\frac{\hbar^2}{2m^*(P)}\left\{\frac{1}{\rho}\frac{\partial}{\partial\rho}\left(\rho\frac{\partial}{\partial\rho}\right)+\frac{\partial^2}{\partial z^2}\right\}N_iJ_0(\alpha\rho)$$
$$\times\cos(\beta z)\exp\{-\lambda[\rho^2+(z-z_i)^2]^{1/2}\} = -\frac{\hbar^2}{2m^*(P)}N_i\exp\{-\lambda[\rho^2+(z-z_i)^2]\}$$
$$\times\left[(-\alpha^2-\beta^2+\lambda^2)J_0(\alpha\rho)\cos(\beta z)-\frac{2\lambda J_0(\alpha\rho)\cos(\beta z)}{[\rho^2+(z-z_i)^2]^{1/2}}+\frac{2\lambda\alpha J_1(\alpha\rho)\rho\cos(\beta z)}{[\rho^2+(z-z_i)^2]^{1/2}}+\frac{2\beta\lambda_z J_0(\alpha\rho)\sin(\beta z)}{[\rho^2+(z-z_i)^2]^{1/2}}\right], \quad (11)$$

where, H_T is the kinetic energy part of the Hamiltonian given in Eq. (1).

The kinetic energy of the donor impurity is thus obtained as,

$$T_h = \int\Psi_i^*(\rho,z)[H_T\Psi_i(\rho,z)]dV = \frac{\hbar^2N^2(\alpha^2+\beta^2-\lambda^2)}{2m^*(P)} + \frac{\lambda\hbar^2N_i^2}{m^*(P)}\int_0^d \rho J_0^2(\alpha\rho)d\rho$$
$$\times\int_0^{(L_z(P)/2)}\frac{\cos^2(\beta z)\exp\{-\lambda[\rho^2+(z-z_i)^2]^{1/2}\}}{[\rho^2+(z-z_i)^2]^{1/2}}dz - \frac{\lambda\alpha\hbar^2N_i^2}{m^*(P)}\int_0^d \rho^2J_1(\alpha\rho)J_0(\alpha\rho)d\rho$$
$$\times\int_0^{(L_z(P)/2)}\frac{\cos^2(\beta z)\exp\{-\lambda[\rho^2+(z-z_i)^2]^{1/2}\}}{[\rho^2+(z-z_i)^2]}dz - \frac{\beta\lambda\hbar^2N_i^2}{m^*(P)}\int_0^d \rho J_0^2(\alpha\rho)d\rho$$

$$\times \int_0^{(L_z(P)/2)} \frac{\cos(\beta z)\sin(\beta z)\exp\{-\lambda[\rho^2+(z-z_i)^2]^{1/2}\}}{[\rho^2+(z-z_i)^2]^{1/2}} z dz. \tag{12}$$

The potential energy for the hydrogenic donor impurity is given by

$$V_h(\rho,z) = -\frac{e^2}{4\pi\varepsilon(0)}\int \Psi_i^*(\rho,z)\left[\frac{1}{(\rho^2+(z-z_i)^2)^{1/2}}\Psi(\rho,z)\right]dV = -\frac{e^2 N_{i,h}^2}{4\pi\varepsilon(0)}\int_0^{2\pi} d\phi \int_0^d \rho J_0^2(\alpha\rho)d\rho$$
$$\times \int_0^{(L_z/2)} \frac{\cos^2(\beta z)\exp\{-2\lambda[\rho^2+(z-z_i)^2]^{1/2}\}}{[\rho^2+(z-z_i)^2]^{1/2}}dz = -\frac{e^2 N_{i,h}^2}{2\varepsilon(0)}\int_0^d \rho J_0^2(\alpha\rho)d\rho$$
$$\times \int_0^{(L_z/2)} \frac{\cos^2(\beta z)\exp\{-2\lambda[\rho^2+(z-z_i)^2]^{1/2}\}}{[\rho^2+(z-z_i)^2]^{1/2}}dz. \tag{13}$$

Thus, the total energy of the donor impurity is given by

$$E_{\text{h,total}} = T_h + V_h \tag{14}$$

2.2. The total energy of the donor in the excited state

The Hamiltonian of the hydrogenic donor impurity in the final state to which the donor is excited is given by

$$H_f = -\frac{\hbar^2}{2m^*(P)}\left\{\frac{1}{\rho}\frac{\partial}{\partial\rho}\left(\rho\frac{\partial}{\partial\rho}\right)+\frac{\partial^2}{\partial z^2}\right\}+V_B(\rho,z), \tag{15}$$

and we have taken the wave function for the donor impurity in this state to be

$$\Psi_f(\rho,z) = N_f J_0(\alpha\rho)\cos(\beta z)\exp(ikz), \tag{16}$$

but in this state, $k = 0$ in the first excited state. Hence the total energy of the donor impurity in this state is

$$E_f = \frac{-\hbar^2}{2m^*(p)}\frac{\int \Psi_f^*[H_f\Psi_f]dV}{\int \Psi_f^*\Psi dV} \tag{17}$$

where $\int \Psi_f^*\Psi dV = 1$ is the normalization condition which yields

$$N_f^2 = \left[\int_0^{2\pi} d\phi \int_0^d \rho J_0^2(\alpha\rho) \int_0^{L_z/2} \cos^2(\beta z)dz\right]^{-1}$$
$$= \left[2\pi \int_0^d \rho J_0^2(\alpha\rho)d\rho \int_0^{L_z/2} \cos^2(\beta z)dz\right]^{-1}. \tag{18}$$

From Eqs. (16) and (17), the total energy of the excited state is found to be

$$E_f = \frac{\hbar^2(\alpha^2+\beta^2)}{m^*(P)} \tag{19}$$

The minimum energy, $E_{\min}$ of the donor impurity is obtained from the expression in Eq. (14), subject to the minimization condition

$$\frac{\partial E_{\text{h, total}}}{\partial\lambda} = 0. \tag{20}$$

The binding energy of the donor impurity is then obtained from the Eqs. (14) and (19). Thus,

$$E_{\text{binding}} = E_f - E_{\min}. \tag{21}$$

2.3. Non-hydrogenic donor impurity

The Hamiltonian for the non-hydrogenic donor impurity is given by

$$H_{n-h} = -\frac{\hbar^2}{2m^*(P)}\left\{\frac{1}{\rho}\frac{\partial}{\partial\rho}\left(\rho\frac{\partial}{\partial\rho}\right)+\frac{\partial^2}{\partial z^2}\right\}$$
$$-\frac{e^2}{4\pi\varepsilon(\rho,z,P)}\frac{1}{[\rho^2+(z-z_i)^2]^{1/2}}+V_B(\rho,z). \tag{22}$$

and the stress-dependent spatial dielectric function is given by

$$\varepsilon(\rho,z,P) = \varepsilon(\rho,z)\exp(\delta P), \tag{23}$$

where, $\delta = -1.73\times10^{-3}$ kbar^{-1} and,

$$\frac{1}{\varepsilon(\rho,z)} = \frac{1}{\varepsilon(0)} + \left(1-\frac{1}{\varepsilon(0)}\right)$$
$$\times \exp\left\{-\frac{1}{c}[\rho^2+(z-z_i)^2]^{1/2}\right\}, \tag{24}$$

is the Hermanson's spatial dielectric function [35] with $c = 5.38 \times 10^{-21}$ nm^{-1}.

The static dielectric constant was taken to be $\varepsilon(0) = 12.56$ [13].

The Hamiltonian for the non-hydrogenic donor impurity now has an additional term, ΔV, in the potential energy operator due to the spatial dielectric function $\varepsilon(\rho, z)$. Here we have also used the same trial wave function as for the hydrogenic donor impurity case. Thus,

$$V_{n-h}(\rho, z) = V_h + \Delta V \tag{25}$$

where V_h is given by Eq. (13) and ΔV is a perturbative term due the spatial dielectric function and is given by

$$\Delta V = -\frac{e^2}{4\pi}\left(1 - \frac{1}{\varepsilon(0)}\right) N_h^2 \int_0^{2\pi} d\phi \int_0^{d} \rho J_0^2(\alpha\rho) d\rho \int_0^{L_z/2} \frac{\cos^2(\beta z) \exp\left\{-\left(\frac{1}{c}+2\lambda\right)[\rho^2+(z-z_i)^2]^{1/2}\right\}}{[\rho^2+(z-z_i)^2]^{1/2}} dz$$

or

$$\Delta V = -\frac{e^2 N_h^2}{2}\left(1 - \frac{1}{\varepsilon(0)}\right) \int_0^{d} \rho J_0^2(\alpha\rho) d\rho \int_0^{L_z/2} \frac{\cos^2(\beta z) \exp\left\{-\left(\frac{1}{c}+2\lambda\right)[\rho^2+(z-z_i)^2]^{1/2}\right\}}{[\rho^2+(z-z_i)^2]^{1/2}} dz. \tag{26}$$

The total energy of the non-hydrogenic donor impurity is thus given by

$$E_{\text{total},n-h} = T_h + V_h + \Delta V. \tag{27}$$

The minimum energy, $E_{\text{total},n-h}$, for the nonhydrogenic donor impurity is obtained by minimizing the above expression with respect to the variational parameter λ.

2.4. Binding energy and photoionization cross-section

In both hydrogenic and non-hydrogenic cases, the binding energy is obtained by subtracting the respective minimum energy from the free energy. The binding energy is then used to obtain the photoionization cross-section from

$$\sigma(\omega, P) = \frac{(4\pi^2\varphi)}{3}\omega \left[\frac{n}{\varepsilon(0)}\right]\left[\frac{\xi_{\text{eff}}}{\xi_0}\right]^2 \times \sum_j |\langle\Psi_f|\vec{z}|\Psi_i\rangle|^2 \delta(E_f - E_i - \hbar\omega). \tag{28}$$

In Eq. (28), $\langle\Psi_f|$ is the final state into which the donor impurity is excited, $|\Psi_i\rangle$ is the ground state trial wave function of both the hydrogenic and non-hydrogenic donor impurities, whichever is the case in the calculation. The constants n and ε are the refractive index and dielectric constant of the GaAs QD material, respectively, and ξ_{eff} is the effective electric field of the incoming radiation on the donor impurity, while ξ_0 is the average field in the medium. In practice, it is not easy to determine ξ_{eff}, hence the effective field ratio ξ_{eff}/ξ_0 is used in the calculation of photoionization cross-section. Since the ratio is not known to affect the shape of the photoionization cross-section, it is generally set equal to unity [36].

In addition, $\varphi = e^2/\hbar c$ is the fine structure constant. The term $\langle\Psi_f|\vec{r}|\Psi_i\rangle$ is the position matrix element of the dipole moment between the two states $\langle\Psi_f|$ and $|\Psi_i\rangle$, where

$$\vec{r} = (\rho\cos\theta)\hat{i} + (\rho\sin\theta)\hat{j} + z\hat{k}. \tag{29}$$

Furthermore, in Eq. (28),

$$\delta(E_f-(E_i+\hbar\omega)) = \frac{\hbar\Gamma}{\pi[(\hbar\omega-(E_f-E_i))^2+(\hbar\Gamma)^2]}. \tag{30}$$

where $\Gamma = 0.1R^*$ is the donor impurity linewidth. Here, $R^* \approx 5.25$ meV is the effective Rydberg energy.

3. Results and discussion

In this section we present our results and discuss their implications. In Fig. 1, we show the variation of the photionization cross-sections of an on-center hydrogenic donor impurity in a cylindrical QD with incident photon frequency for quantum

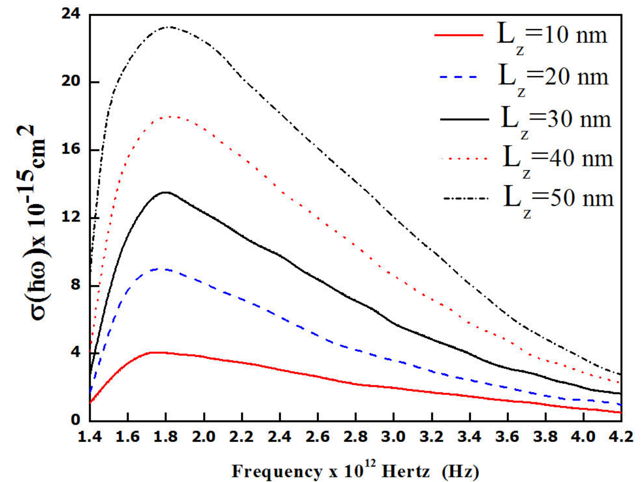

FIGURE 1. Variation of photoionization cross-section of an on center shallow hydrogenic donor impurity in a cylindrical quantum well dot with incident photon frequency for quantum dot side lengths $L_z = 10$, 20, 30, 40 and 50 nm.

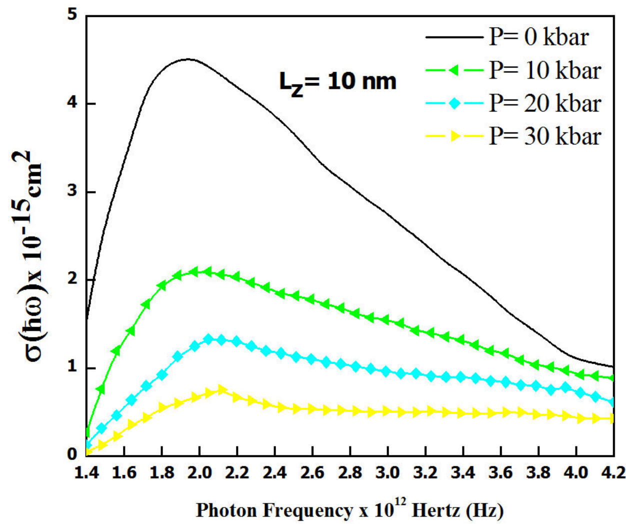

FIGURE 2. Variation of photoionization cross-section of an on-center shallow hydrogenic donor impurity with incident photon frequencies for four constant values of uniaxial stress, $P = 0$, 10, 20, and $P = 30$ kbars applied along the z axis of the quantum dot; and for quantum dot side length $L_z = 10$ nm.

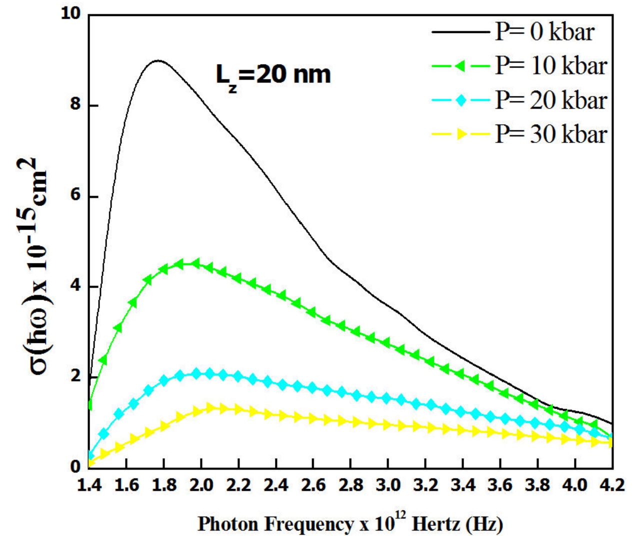

FIGURE 3. Variation of photoionization cross-section of an on-center shallow hydrogenic donor impurity with incident photon frequencies for four constant values of uniaxial stress, $P = 0$, 10, 20, and $P = 30$ kbars applied along the z axis of the quantum dot; and for quantum dot side length $L_z = 20$ nm.

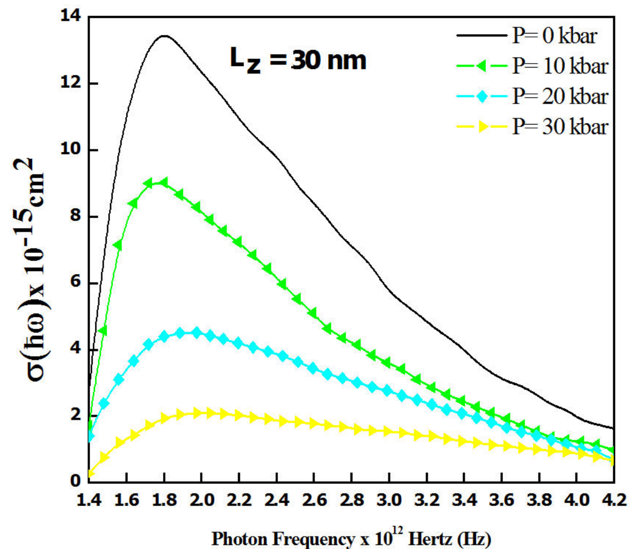

FIGURE 4. Variation of photoionization cross-section of an on-center shallow hydrogenic donor impurity with incident photon frequencies for four constant values of uniaxial stress, $P = 0$, 10, 20, and $P = 30$ kbars applied along the z axis of the quantum dot; and for quantum dot side length $L_z = 30$ nm.

dots of axial lengths, $L_z = 10$, 20, 30, 40 and 50 nm. We observe that, for all the axial lengths and constant radius of the QD, the photoionization cross-section rises from some miminum ranging from $\sigma(\omega) = 1.78 \times 10^{15}$ cm^2 at $f = 1.4 \times 10^{12}$ Hz to a maximum of $\sigma(\omega) = 4 \times 10^{15}$ cm^2 at $f = 1.7 \times 10^{12}$ Hz for $L_z = 10$ nm (the solid, red curve), from a minimum of $\sigma(\omega) = 10 \times 10^{15}$ cm^2 at $f = 1.4 \times 10^{12}$ Hz to a maximum of $\sigma(\omega) = 23.5 \times 10^{15}$ cm^2 at $f = 1.8 \times 10^{12}$ Hz QD length of $L_z = 50$ nm (dash-dotted, black curve) for the largest photoionization cross-section. It can also be observed that all the peaks of the photoionization cross-sections cluster around an incident frequency of about $f = 1.8 \times 10^{12}$ Hz. Thereafter, the photoionization cross-sections decrease steeply at first and then gradually to some constant values which are close to each other as the incident photon frequency increases beyond $f = 4.2 \times 10^{12}$ Hz . It seems that the photoionization cross-section becomes less sensitive to further increase of incident photon frequency beyond this particular frequency regime.

In Fig. 2, the variation of the photoionization cross-section of an on-center hydrogenic donor impurity with uniaxially applied stress for a range of incident photon frequencies is shown. Specifically, we have used for the applied stress, $P = 0$, 10, 20, 30 kbars on a QD of constant length of 10 nm. We observe that for the same frequency range, the photoionization cross-sections of the donor impurity increase from a low value to a peak and then it decreases as the frequency increases beyond $f = 2.0 \times 10^{12}$ Hz until it reaches a constant value from about $f = 4.2 \times 10^{12}$ Hz. From this frequency and beyond, the photoionization cross-section appears to be independent of the frequency. It is also noted that for the same QD length, the photoionization increases with decreasing applied stress. For example, the peak of the photoionization cross-section of the donor impurity with no applied stress is almost four times that for $P = 30$ kbar at almost the same frequency.

From Fig. 3, it is observed that for a constant length of $L_z = 20$ nm, the photoionization cross-sections follow the same trend observed for $L_z = 10$ nm, except that the photionization cros-sections are much larger with the highest peak reaching $\sigma(\omega) = 9 \times 10^{-15}$ cm^2 for $P = 0$ kbar and $\sigma(\omega) = 4.3 \times 10^{-12}$ cm^2 for $P = 10$ kbar. These values of the cross-sections are almost twice the values observed for

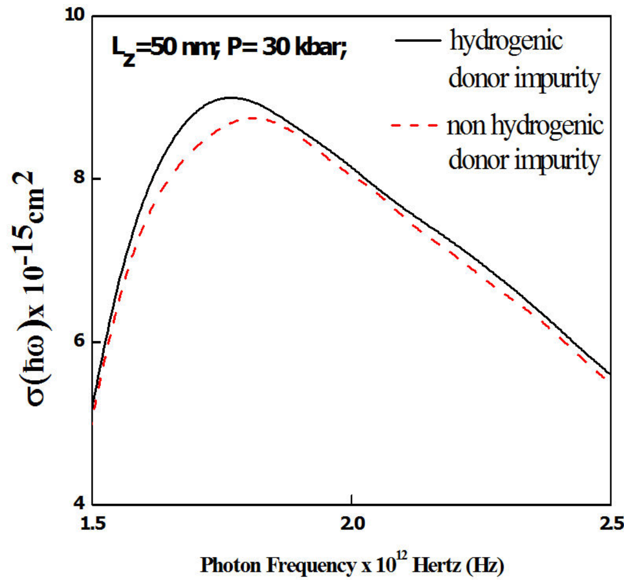

FIGURE 5. Variation of photoionization cross-section of an on-center shallow hydrogenic donor impurity and non hydrogenic donor impurity with incident photon frequencies for a fixed value of uniaxial stress, $P = 30$ kbar applied along the z axis of the quantum dot; and for quantum dot side length $L_z = 50$ nm.

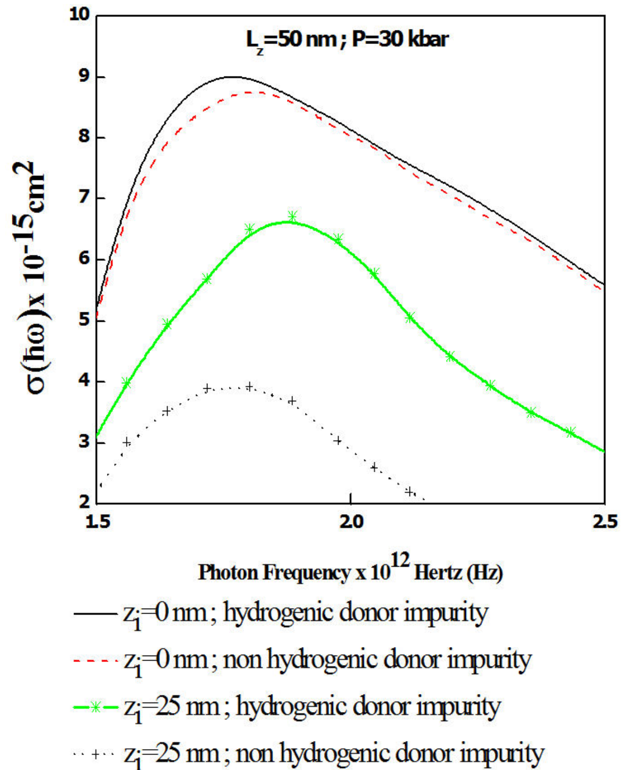

FIGURE 6. Variation of photoionization cross-section of hydrogenic donor impurity and non hydrogenic donor impurity with incident photon frequencies for a fixed value of uniaxial stress, $P = 30$ kbar applied along the z axis of the quantum dot; and for quantum dot side length $L_z = 50$ nm.

the QD of length $L_z = 10$ nm. Figure 4 also shows the same trend observed for Figs. 2 and 3, *i.e.*, that as the length of the QD increases, with other parameters kept constant, the photoionization cross-section are much larger for $P = 0$ kbar and decreases with increasing applied stress for constant QD size. This means that applied stress suppresses the photoionization cross-section of the donor impurity.

In Fig. 5, we compare the effect of applied uniaxial stress of $P = 30$ kbar on the photoionization cross-section for both hydrogenic and non-hydrogenic donor impurity on a QD of length $L_z = 50$ nm and radius $r = 5$ nm. Initially, there is no difference on the photoionization cross-sections for the hydrogenic and non-hydrogenic donor inpurities with incident photon frequency until about $f = 1.5 \times 10^{12}$ Hz when there is a clear difference in the effect of the applied stress to the photoionization cross-sections with the effect being more pronounced in the non-hydrogenic case than in the hydrogenic case. This effect on the cross-section reaches its peak at about $f = 1.7 \times 10^{12}$ Hz. Thereafter, the photoionization cross-sections decrease gradually towards some minima at which any further increase in incident photon frequency does not affect the photoionization cross-section.

Finally, in Fig. 6, we present the plots of the photoionization cross-sections for two donor impurity positions along the z-axis and with incident photon frequency varying from $f = 1.5 \times 10^{12}$ Hz to $f = 2.5 \times 10^{12}$ Hz for a constant applied uniaxial stress $P = 30$ kbar, and for a QD of radius $r = 5$ nm, and length $L_z = 50$ nm. We observe that for on center donor impurities, the photoionization cross-sections of the hydrogenic and non-hydrogenic donors are close to each other while for the donor impurities located at $z_i = 25$ nm, the photoionization cross-section of the hydrogenic donor impurity is much greater than that of the non-hydrogenic one throughout the frequency range considered.

4. Conclusions

We have used a variational technique within the effective mass approximation to study the variation of the photoionization cross-section of a hydrogenic and a non-hydrogenic donor impurity in a GaAs quantum dot with incident photon frequency and applied uniaxial stress. The quantum dot is of a cylindrical geometry and the donor impurity is located at various positions along the axis of the quantum dot. In our study, we have observed that for both hydrogenic and non-hydrogenic donor impurity the photoionization cross-section increases rapidly with incident photon frequency from some low value, up to a peak of about the same cluster of frequency then it decreases with further increase in frequency up to a point where the photoionization is no longer sensitive to the incident photon frequency. This is true for all positions of the donor impurities and lengths of the QD we studied.

However, the photoionization cross-sections for longer QD are much larger than those for smaller QDs in both the hydrogenic and non-hydrogenic donor impurity cases. We have observed that the applied uniaxial stress depresses the

photoionization cross-sections in both hydrogenic and non-hydrogenic donor impurity cases. Importantly, the photoionization cross-sections for the hydrogenic donor impurity are larger than for the non-hydrogenic donor impurity for the same incident photon frequencies, QD size, and same applied uniaxial stress. The study has, therefore, shown that the photoionization cross-sections of hydrogenic and non-hydrogenic donor impurities are different for the same quantum dot size, the same incident photon frequencies, and same applied uniaxial stress. Furthermore,the larger the QD, the larger is the photoionization cross-section. It is our conclusion that when designing thermo-electronic and opto-electronic devices using GaAs QDs one should take into consideration the frequency at which the photoionization is optimum, whether or not the donor impurity is of hydrogenic or non-hydrogenic type. Consideration should also be taken of the stresses to which the device will be subjected to, for example, a device which will be used in a fighter aircraft will be subjected to very high and sudden g-forces and hence must be robust enough to withstand these forces.

1. J. R. Arthur, *Sur. Sci.* **500** (2002).
2. A. Y. Cho, *J. Appl. Phys.* **42** (1971) 2074.
3. E. H. C. Parker, *Technology and Physics of Molecular Beam Epitaxy* (Plenum Press, New York, 1985).
4. D. K. Kerry, *Gallium Arsenide Technology* (H. W. Sama, Michigan, 1985).
5. H. L. Manasevit, *J. Electrochem. Soc.* **118** (1971) 647.
6. H. C. Casey and B.N. Panish, *Heterostructures and Lasers* (Academic Press, New York, 1978) Part A.
7. R. Dingle, In *Festkörperprobleme, Münster*, edited by H. J. Quessner (Pergamon Press, Braunschweig, 1975), Vol. **15**, p. 21.
8. P. C. Sercel and K. J. Vahala, *Phys. Rev. B* **42** (1990) 3690.
9. H. Odhiambo Oyoko, *Phys. Scr.* **66** (2002) 94-96.
10. C. A. Duque, N. Porrass-Montenegro and H. Oyoko, *Rev. Colomb. Fis.* **34** (2002).
11. H. O. Oyoko, C. A. Duque and N. Porrass-Montenegro, *J. Appl. Phys* **90** (2001) 819-823.
12. G. Bastard, *Phys. Rev B* **24** (1981) 4714.
13. P. Csavinszky and H. Oyoko, *Phys. Rev B* **43** (1991) 9262.
14. P. Csavinszky and A. M Elabsy, *Phys. Rev B* **32** (1985) 6498.
15. J. Lee and H.N. Spector, *Journal of Vacuum Sci. Technol.B* **2** (1984) 16.
16. J. W. Brown and H. N. Spector, *Journal of Applied Physics* **59** (1986) 1179.
17. Heon Ham and H. N. Spector, *Journal of Appl. Phys* **93** (2003) 3900.
18. E. Feddi, M. El-Yadri, F. Dujardin, R. L. Restrepo, and C. A. Duque, *J. Appl. Phys* **121** (2017) 064303.
19. A. Sali and H. Satori, *Superlattices and Microstructures*, **69** (2014) 38-52.
20. E. Kasapoglu, U. Yesilgul, H. Sari, and I. Sokmen, *Physica B* **368** (2005) 76-81.
21. E. Kasapoglu, H. Sari, U. Yesilgul and I. Sokmen, *J. Phys.:Condens.Matter* **18** (2006) 6263-6271.
22. M. G. Barseghyan, A. A. Kirakosyan, and C. A. Duque, *Phys.Stat.sol(b)* **246** (2009) 626-629.
23. H. Ham and H. N. Spector, *J. Appl. Phy* **100** (2006) 024304.
24. H. Ham and C. J. Lee, *J. Korean Phys. Soc.*, **42** (2013) S289.
25. E. Iqraoun *et al., Philosophical Magazine* **97** (2017) 1445-1463.
26. F. Oketch , H. Oyoko and G. Amolo, *J. Korean Phys. Soc*. **73** (2018) 928-933.
27. J. D. Correa N. Porras-Montenegro and C. A. Duque, *Physica Stat. Solidi* **241** (2004) 2440.
28. I-H. Lee Y. J. Park, D. Kim, Y. H. Jeong, and K.-B. Lee, *Phys. Rev. B* **57** (1998) 9035.
29. K. Hirose and N. S. Wingreen, *Phys. Rev. B* **59** (1999) 4604.
30. I-H. Lee K. H. Ahn, Y.H. Kim, R. M. Martin, and J. P. Leburton, *Phys. Rev. B* **60** (1999) 13720.
31. B. Welber, M. Cardona, C. K. Kim, and S. Rodriguez, *Phys. Rev. B* **12** (1975) 5729.
32. D. E. Aspnes, *Phys. Rev. B* **14** (1976) 5331.
33. S. Adachi, *J. Appl. Phys*. **58** (1985) R1.
34. M.E. Mora-Ramos, S. Y. Lopez and C. A. Duque, *Eur. Phys. J. B* **62** (2008) 257-261.
35. J. Hermanson *Phys. Rev. B* **150** (1966) 660.
36. M. Lax, *In Proceedings* of (1954) proceedings of Conference Held at Atlantic City, Atlantic City, edited by R. G. Breckenridge (Wiley, New York 1956), p. 11.